

Geochemical zones and environmental gradients for soils from the Central Transantarctic Mountains, Antarctica

Melisa A. Diaz^{1,2†*}, Christopher B. Gardner^{1,2}, Susan A. Welch^{1,2}, W. Andrew Jackson³, Byron J. Adams⁴, Diana H. Wall⁵, Ian D. Hogg^{6,7}, Noah Fierer⁸, W. Berry Lyons^{1,2}

¹School of Earth Sciences, The Ohio State University, Columbus, OH, USA

²Byrd Polar and Climate Research Center, The Ohio State University, Columbus, OH, USA

³Department of Civil, Environmental, & Construction Engineering, Texas Tech University, Lubbock, TX, USA

⁴Department of Biology, Evolutionary Ecology Laboratories, and Monte L. Bean Museum, Brigham Young University, Provo, UT, USA

⁵Department of Biology and School of Global Environmental Sustainability, Colorado State University, Fort Collins, CO, USA

⁶Canadian High Arctic Research Station, Polar Knowledge Canada, Cambridge Bay, Nunavut, Canada

⁷School of Science, University of Waikato, Hamilton, New Zealand

⁸Department of Ecology and Evolutionary Biology and Cooperative Institute for Research in Environmental Science, University of Colorado Boulder, Boulder, CO, USA

[†]Now at [Departments of Geology and Geophysics and Applied Ocean Physics and Engineering, Woods Hole Oceanographic Institution, Woods Hole, MA, USA](#)

Correspondence to: Melisa A. Diaz (diaz.237@osu.edu/diaz@whoi.edu)

Abstract. Previous studies have established links between biodiversity and soil geochemistry in the McMurdo Dry Valleys, Antarctica, where environmental gradients are important determinants of soil biodiversity. However, these gradients are not well established in the Central Transantarctic Mountains, which are thought to represent some of the least hospitable Antarctic soils. We analyzed 220 samples from 11 ice-free areas along the Shackleton Glacier (~85 °S), a major outlet glacier of the East Antarctic Ice Sheet. We established three zones of distinct geochemical gradients near the head of the glacier (upper), central (middle), and at the mouth (lower). The upper zone had the highest water-soluble salt concentrations with total salt concentrations exceeding 80,000 $\mu\text{g g}^{-1}$, while the lower zone had the lowest water-soluble N:P ratios, suggesting that, in addition to other parameters (such as proximity to water/ice), the lower zone likely represents the most favorable ecological habitats. Given the strong dependence of geochemistry with-on geographic parameters, we established developed multiple linear regression and random forest models to predict soil geochemical trends given latitude, longitude, elevation, distance from the coast, distance from the glacier, and soil moisture (variables which can be inferred from remote measurements). Confidence in our random forest model predictions was moderately high, with R^2 values for total water-soluble salts, water-soluble N:P, ClO_4^- , and ClO_3^- of 0.851, 0.8842, 0.7840, and 0.7428, respectively. These modeling results can be used to predict geochemical gradients and estimate salt concentrations for other Transantarctic Mountain soils, information that can ultimately be used to better predict distributions of soil biota in this remote region.

1. Introduction

From an ecological standpoint, the least biologically diverse terrestrial systems are those found in extreme physical and chemical environments. The abundance and diversity of life in soils is dependent on a number of environmental variables/parameters, including temperature, precipitation, organic matter content, and nutrient availability (Wall et al., 2012). Hot deserts are typically viewed as one of the least biologically diverse environments. However, but cold deserts can often be even less diverse (Freckman and Virginia, 1998). Soils in Antarctica typically serve as end-members for low habitat suitability due to their high salt concentrations, low organic carbon, low soil moisture, and low mean annual temperatures (Courtright et al., 2001).

In the McMurdo Dry Valleys (MDV), organic matter and salt concentrations influence soil communities, where soils with higher amounts of organic carbon, lower water-soluble N:P ratios, and lower total water-soluble salt concentrations generally harbor the greatest biomass and biodiversity (Barrett et al., 2006; Bottos et al., 2020; Caruso et al., 2019; Magalhães et al., 2012). These Antarctic ecosystems are relatively simple and are among the only known few known soil systems where nematodes and microarthropods (Collembola, Acari) are at the top of the food chain (Freckman and Virginia, 1998; Hogg and Wall, 2012). Studies of soils in the MDV and Transantarctic Mountains (TAM) have been key to understanding ecosystem structure and function in extreme terrestrial environments (e.g. Caruso et al., 2019; Collins et al., 2019, 2020; Convey and McInnes, 2005; Freckman and Virginia, 1998; Hodgson et al., 2010).

Biological processes in Antarctic soils are largely dependent on the availability, duration, and proximity of soils to liquid water (Barrett et al., 2006). Due to the seasonality in freezing and of thawing events, liquid water acts as a pulse to the ecosystem, providing water for organisms, but also wetting surface soils and dissolving soluble salts (Webster-Brown et al., 2010; Zeglin et al., 2009). Experiments of salt thresholds on Antarctic nematodes found that no individuals survived in highly saline soils over (~2,600 mg L⁻¹ TDS) (Nkem et al., 2006). Concentrations of soluble salts exist at these concentrations or higher for at high elevation and inland locations in the TAM (Bockheim, 2008; Lyons et al., 2016). Additionally, studies on TAM soils have found that increased salt concentrations lead to a decrease in soil biodiversity in older soils compared to younger soils (Magalhães et al., 2012). Yet, despite these inhospitable conditions (e.g. high salt concentrations and glacial advance and retreat), some organisms are postulated to have found suitable refugia in TAM soils and persisted in isolation for millions of years and through glacial cycles (Beet et al., 2016; Collins et al., 2019, 2020; Stevens et al., 2006; Stevens and Hogg, 2003).

It is generally accepted that habitat suitability for invertebrate species in Antarctic soils is driven by a combination of geochemical, geographic, hydrologic, and geomorphic variables (Bottos et al., 2020; Courtright et al., 2001; Freckman and Virginia, 1998; Magalhães et al., 2012). Geographic variables, such as elevation, can be measured with advanced mapping tools and satellite imagery; however, surface exposure ages, soil geochemistry and nutrient content require extensive logistical support and resource allocation for sample collection and analysis. More efficient estimation tools

69 ~~better understanding of the relationship between geographic variables and on-the-ground measurements are~~ needed to aid
70 in our ability to understand and predict habitat suitability for invertebrates throughout the TAM.

71 With this study, we determined and evaluated geochemical patterns and gradients of water-soluble ions in soils
72 collected from 11 ice-free areas along the Shackleton Glacier, Central Transantarctic Mountains (CTAM). Particular
73 attention was given to total water-soluble salt concentrations, N:P ratios, and ClO_4^- and ClO_3^- concentrations, based on their
74 influence on biodiversity, as determined in previous studies (e.g. Ball et al., 2018; Barrett et al., 2006b; Courtright et al.,
75 2001; Dragone et al., 2020; Nkem et al., 2006). The geochemical data were compared to geographic parameters to
76 understand how the physical environment influences the observed geochemical variability. Our results show that water-
77 soluble ion concentrations and distributions are driven largely by soil geography and surface exposure age. Finally, we
78 implemented statistical and machine learning techniques to interpolate and predict the soil geochemistry across the region
79 using geographic variables. Our multiple linear regression and random forest models show that latitude, longitude, elevation,
80 distance from the coast, distance from the glacier, and soil moisture (all variables currently or soon to be remotely
81 measurable using maps and satellites) are moderately effective at estimating spatial patterns in TAM soil geochemistry, with
82 R^2 values as high as 0.87. These data will be particularly useful for ecologists seeking to understand refugia and habitat
83 suitability in Antarctica and similarly harsh, desert environments.

84 2. Study sites

85 The Shackleton Glacier (~84.5 to 86.4°S; ~130 km long and ~10 km wide) is a S-N trending outlet glacier of the
86 East Antarctic Ice Sheet (EAIS) located to the west of the Beardmore Glacier and flows through the Queen Maud Mountains
87 (CTAM) into the Ross Sea (Fig. 1). The elevations of exposed soils range from ~150 m.a.s.l. to >3,500 m.a.s.l. from the
88 coast towards the Polar Plateau. Long-term climate data are not yet available, but the Shackleton Glacier region is a polar
89 desert regime, similar to the Beardmore Glacier region, with average annual temperatures well below freezing and little
90 precipitation (LaPrade, 1984).

91 During the Last Glacial Maximum (LGM) and glacial periods throughout the Pleistocene, the size and thickness of
92 the EAIS ~~has been suggested to be~~ was likely greater than current levels (Golledge et al., 2013; Nakada and Lambeck, 1988;
93 Talarico et al., 2012; Wilson et al., 2018). Outlet glaciers, such as the Shackleton Glacier, may have had the greatest
94 increases in extent, especially ~~towards~~ at the glacier terminus (Golledge et al., 2012; Golledge and Levy, 2011). The
95 behavior of local alpine and tributary glaciers is not well-constrained, but these glaciers are also believed to have advanced
96 and retreated over the last two million years (Diaz et al., 2020a; Jackson et al., 2018). As a result, currently exposed soils
97 were overlain and reworked by fluctuations of the Shackleton Glacier and other tributary and alpine glaciers in the region.
98 Exposure ages range from the early Holocene to the Miocene, and generally increase with distance from the coast and
99 distance from the glacier (Balter-Kennedy et al., 2020; Diaz et al., 2020a).

100 The soils contain a range of water-soluble salts derived primarily from atmospheric deposition and chemical
101 weathering (Claridge and Campbell, 1968; Diaz et al., 2020b). The major salts are typically nitrate and sulfate salts,
102 especially at higher elevations and further inland from the coast of the Ross Sea (Diaz et al., 2020b). The solubilities of the
103 salts vary, but nitrate salts are highly soluble and their occurrence at high elevation and inland locations suggests that those
104 soils have maintained persistent arid conditions.

105 3. Methods

106 3.1. Sample collection and preparation

107 During the 2017-2018 austral summer, 220 surface soil samples (~top 5 cm) were collected from 11 distinct ice-free
108 areas (Roberts Massif, Schroeder Hill, Mt. Augustana, Bennett Platform, Mt. Heekin, Thanksgiving Valley, Taylor Nunatak,
109 Mt. Franke, Mt. Wasko, Nilsen Peak, and Mt. Speed) along the Shackleton Glacier, including a subset of 27 samples
110 previously analyzed for S, N, and O isotopes in nitrate and sulfate (Diaz et al., 2020b). At each area, we collected samples in
111 transects (ranging from ~200 m to ~2,000 m in length) to maximize the geochemical variability. Our transects were also
112 designed to capture the LGM transition, with some soils exposed throughout the LGM and others exposed following glacier
113 retreat. GPS coordinates and elevations were recorded with each sample and later used to estimate the distance from coast
114 and distance from the glacier (defined as linear distance from the nearest glacier – Shackleton, tributary, or alpine). Once
115 collected, the samples were stored and shipped frozen (-20 °C) to The Ohio State University.

116 Prior to geochemical analysis, the samples were dried at 50 °C for at least 72 hours with the loss in mass attributed
117 to soil moisture content. The dried soils were leached at a 1:5 soil to DI water ratio, and the leachate was filtered through 0.4
118 µm Nucleopore membrane filters (Diaz et al., 2018, 2020b; Nkem et al., 2006). Due to the low sediment to water ratio, this
119 leaching technique only dissolves the more water-soluble salts (Toner et al., 2013). These include salts with ClO_4^- , NO_3^- , Cl^- ,
120 SO_4^{2-} , ClO_3^- , and $\text{CO}_3^{2-} + \text{HCO}_3^-$. Process blanks were generated and analyzed to account for any contamination from the
121 leaching process.

122 3.2. Analytical analysis of water-soluble anions, cations, and nutrients

123 The analytical techniques used here are similar to those reported by Diaz et al. (2020b). In brief, the analytes
124 included anions (F^- , Cl^- , Br^- , and SO_4^{2-}) which were measured on a Dionex ICS-2100 ion chromatograph, cations (K^+ , Na^+ ,
125 Ca^{2+} , Mg^{2+} , and Sr^{2+}) which were measured on a PerkinElmer Optima 8300 Inductively Coupled Plasma-Optical Emission
126 Spectrometer (ICP-OES), and nutrients ($\text{NO}_3^- + \text{NO}_2^-$, PO_4^{3-} , H_4SiO_4 , and NH_3) which were measured on a Skalar San++
127 Automated Wet Chemistry Analyzer at The Ohio State University. Perchlorate (ClO_4^-) and chlorate (ClO_3^-) were measured
128 using an ion chromatograph-tandem mass spectrometry technique (IC-MS/MS) at Texas Tech University (Jackson et al.,
129 2012, 2015). All analytes are reported as listed. Total water-soluble salt concentration was calculated as the sum of all
130 measured cations and anions. The precision of replicated check standards and samples was typically better than 10% for all
131 major anions, cations and nutrients, and better than 20% for perchlorate and chlorate. Accuracy was typically better than 5%

132 for all major anions, cations, and nutrients, as determined by the NIST 1643e external reference standard and the 2015 USGS
133 interlaboratory calibration standard (M-216), and better than 10% for perchlorate and chlorate, as determined by spike
134 recoveries. Precision and accuracy for individual analytes are located in Table S1. Detection limits for the analytes have been
135 previous reported (Diaz et al., 2018; Jackson et al., 2012).

136 3.3. Data interpolation and machine learning

137 Inverse distance weighted (IDW) interpolations were performed for Bennett Platform, Thanksgiving Valley, and
138 Roberts Massif using the Geostatistical Analyst tool in ArcMap 10.3. Since IDW is a deterministic method where unknown
139 values are predicted based on proximity to known values, we chose those three sites as they had the most defined transects
140 and relatively higher sample density. The interpolation parameters were constant with a power of 4, maximum neighbors of
141 15, minimum neighbors of 5, and 4 sectors, and a variable search radius. These parameters were chosen such that they
142 optimize for the lowest mean absolute error.

143 Multiple linear regressions were generated for all geochemical analytes, except H_4SiO_4 (total of 15 dependent
144 variables), with latitude, longitude, elevation, distance from the coast, distance from the glacier, and soil moisture as
145 independent variables using built-in functions in R 3.6.3 (R Core Team, 2020). Random forest regression models were
146 similarly generated using the randomForest library. The random forest model is a machine learning algorithm that utilizes
147 supervised learning algorithms to predict values given input predictor variables (Breiman, 2001). Multiple decision trees are
148 run in parallel with a randomized subset of predictor variables, and the aggregate result of each tree is used to generate a
149 predicted outcome. Since each tree is generated using a random sample and random predictor variables, the random forest
150 model is effective at minimizing overfitting and handling outliers (Breiman, 2001). [For both models, all geochemical data
151 were log-transformed to ensure the data were normally distributed \(verified using a Jarque-Bera normality test\). Missing
152 values were input as NA.](#)

153 Machine learning algorithms are widely used in variety of disciplines from finance (Patel et al., 2015) to ecology
154 (Davidson et al., 2009; Peters et al., 2007; Prasad et al., 2006), for both data prediction (regression) and classification.
155 Recently, these techniques have been used for Earth Science applications, including geologic mapping (Heung et al., 2014;
156 Kirkwood et al., 2016), air quality monitoring (Stafoggia et al., 2019), and water contaminant tracing (Tesoriero et al., 2017).
157 We developed a novel application of machine learning to predict concentrations and gradients of water-soluble salts in
158 Antarctic soils, given set geographic parameters, similar to the approaches developed for stock market and real estate
159 predictions (Antipov and Pokryshevskaya, 2012; Patel et al., 2015).

160 For our random forest models, any sparse missing values in Table S2 were estimated by averaging the geochemistry
161 of the samples collected immediately before and after in the same transect. Missing values due to concentrations below the
162 detection limit were input as [QNA](#). The new imputed dataset was split into a training set representing 86% of the data ($n =$
163 189, Table S3) and a testing set representing the remaining 14% ($n = 31$, Table S4), [based on ideal model parameters](#)

164 [described by Breiman \(2001\)](#). The training dataset was used to generate the random forest models for each analyte. Each of
165 the models were run with 2000 decision trees (ntree = 2000) to minimize the mean squared errors. The number of random
166 variables used for each node split in the decision trees was set to the recommended regression default of variables/3 to
167 optimize the model randomness, which in our case was 2 (mtry = 2), following parameters described previously (Breiman,
168 2001). The scripts developed for both the multiple linear regression and random forest models are included in the
169 supplementary materials.

170 4. Results

171 4.1. Geochemistry of upper, middle, and lower zones

172 The maximum, minimum, mean, standard deviation and coefficient of variation are reported in Table 1 for the
173 measured geographic and geochemical data. Concentrations of water-soluble ions span up to five orders of magnitude and
174 are variable across the region. Elevation, distance from the coast, distance from the glacier, and soil moisture are also
175 variable and span up to three orders of magnitude. The highest elevation samples (> 2,000 m.a.s.l.) were collected from
176 Schroeder Hill and the greatest soil moisture content is from Mt. Wasko at 12.3%, with a mean of 2.1% for all samples.

177 Shackleton Glacier region surface soils can be separated into three zones based on their water-soluble geochemistry:
178 an upper zone near the Polar Plateau, a middle zone near the center of the glacier, and a lower zone where the glacier flows
179 into the Ross Sea (Figs. 1; 2). The upper zone samples are characterized by the highest total water-soluble salt
180 concentrations, with the highest values greater than 80,000 $\mu\text{g g}^{-1}$ at Schroeder Hill, while the lower zone samples have the
181 lowest total salt concentrations, with the lowest values near 10 $\mu\text{g g}^{-1}$ at Mt. Wasko (Fig. 2a-c). The middle zone has
182 intermediate values. Water-soluble N:P molar ratios generally follow a similar trend (Fig. 2d-f). The lowest N:P ratios are in
183 the lower zone soils, while the middle and upper zones have more variable values. Concentrations of ClO_4^- and ClO_3^- follow
184 similar trends as the total salts, with less distinction between middle and upper zones, though most concentrations in the
185 lower zone are below the detection limit (Fig. 2g-l; Table S2).

186 Observed trends between the zones appear to be driven, at least partially, by geography. Regressions of total water-
187 soluble salt concentration, water-soluble N:P ratio, and ClO_3^- concentration with elevation, distance from the coast, and
188 distance from the glacier are all positive (Fig. 2). The strongest relationships are between total salts and elevation, and ClO_3^-
189 N:P ratio and distance from the coast/elevation, with R^2 values of 0.5926 and 0.5224, respectively, and p-values < 0.001 with
190 a Bonferroni Correction, which was applied to minimize the familywise type 1 error rate associated with multiple
191 comparisons (Fig. 2a; 2dk). The weakest relationships are between $\text{ClO}_4^-/\text{ClO}_3^-$ and distance from the coast, and ClO_3^- and
192 distance from the glacier, with R^2 values of 0.011 and 0.06, respectively (Fig. 2h; 2i). Distance from the glacier varies
193 widely between individual zones with frequent overlaps, but there appears to be a moderate relationship with N:P ratio and
194 total salts (Fig. 2c; 2f). Overall, total salt concentration has the strongest relationship with geography and ClO_4^- has the
195 weakest relationships.

196 Ternary diagrams highlight the specific geochemical gradients within and between the zones. The anion ternary
197 diagram only includes SO_4^{2-} , NO_3^- , and Cl^- , which are the major water-soluble salts in the region (Claridge and Campbell,
198 1968; Diaz et al., 2020b). Though carbonate and bicarbonate salts have been identified in both lacustrine sediments and soils
199 in Antarctica, previously measured concentrations in the Shackleton Glacier region were low, ranging from 0.07 to 2.5%,
200 and bicarbonate salts were not identified in the highest elevation and furthest inland soils (Claridge and Campbell, 1968;
201 Diaz et al., 2020b; Lyons et al., 2016). The most abundant anion for the upper zone is SO_4^{2-} , which is greater than 99% of the
202 total anion budget in some Schroeder Hill and Roberts Massif samples, though other locations are dominated by NO_3^- (Fig.
203 3). The anions are more evenly distributed in the middle zone, though the majority of samples are most abundant in NO_3^- and
204 Cl^- . The lower zone has much lower SO_4^{2-} fractions than the upper zone and the dominant anion is generally Cl^- . The cation
205 distribution is very similar for all three zones (Fig. 3). $\text{Na}^+ + \text{K}^+$ is the most abundant cation pair representing over 90% of
206 the total cations for many upper and middle zone samples, while Ca^{2+} is the second most abundant. In general, Mg^{2+} is the
207 least abundant cation across all sampling locations.

208 4.2. Statistical geochemical variability

209 A principal component analysis (PCA) [using the correlation matrix \(i.e. scale = TRUE\)](#) was performed in R (using
210 factoextra (Kassambara and Mundt, 2017) and built in R software libraries) to determine which geochemical variables most
211 strongly differ across the samples. For the PCA, the first two principal components account for over 50% of the total dataset
212 variability at 44.2% and 11.6%, respectively. The different zones are correlated with different principal components (Fig. 4).
213 The samples from the middle zone are positively correlated with PC1 and PC2. In the biplot, they plot in the upper right
214 quadrant with high concentrations of Cl^- , NO_3^- , water soluble N:P ratio, and Ca^{2+} , with a minor influence from soil moisture
215 and H_4SiO_4 . The upper zone samples generally plot along PC1 and are most associated with Sr^{2+} , SO_4^{2-} , Mg^{2+} , Na^+ , K^+ , F^- ,
216 ClO_4^- , and ClO_3^- . The samples from the lower, more coastal zone are negatively correlated with PC1 and are distinguished by
217 their higher PO_4^{3-} concentrations. Most samples from all locations plot within the 95% confidence interval ellipses.
218 However, there are two strong outliers from Schroeder Hill and Mt. Heekin.

219 Similar to the PCA, we performed a simple Spearman's rank correlation for the entire dataset to visualize the
220 statistical dependence between all variables. Since a goal of this study is to relate water-soluble ion concentrations to
221 geography, we focused on latitude, longitude, distance from the coast, distance from the glacier, and soil moisture. The
222 strongest correlation coefficients are between Cl^- and latitude, elevation, and distance from the coast, and Sr^{2+} and soil
223 moisture (Fig. 5). Most other correlations are moderate to weak, though there appear to be notably stronger correlations
224 between ClO_3^- and latitude and distance from coast, Ca^{2+} and longitude, elevation, and distance from coast, NO_3^- and
225 latitude, and SO_4^{2-} with distance from glacier. Longitude, elevation, and distance from coast have the greatest number of
226 strong and moderate correlations with the geochemistry data. Outside of the geographic parameters, Na^+ is highly correlated
227 with total water-soluble salts, likely representative of the high $\text{Na}^+ + \text{K}^+$ percentages (Fig. 3), and Sr^{2+} is highly correlated
228 with K^+ , likely reflecting a common ion source.

4.3. Spatial interpolation and machine learning model performance

The total salt concentrations of individual samples at Bennett Platform produce the most defined interpolation gradient from the glacier front to further inland compared to Roberts Massif and Thanksgiving Valley (Fig. 6). Bennett Platform also has the smoothest salt concentration contours suggesting that the interpolation model is the strongest and most robust at this location. The second strongest interpolation is Thanksgiving Valley. Contrary to the measurements at Bennett Platform, Thanksgiving Valley has the highest salt concentrations in the center of the valley, with lower concentrations to both the east and west. The lowest concentration contours are closest to the glacier for both Bennett Platform and Thanksgiving Valley, which is likely related to glacial history since the soils near the glacier are relatively younger than those further inland based on meteoric ^{10}Be data (Diaz et al., 2020a). The interpolation from Roberts Massif does not have a distinguishable spatial trend.

The multiple linear regression and random forest models vary in their strength for the individual analytes. The highest R^2 value from the linear regression is 0.655 for NaSr^{2+} , while total water-soluble salts, water-soluble N:P ratio, ClO_4^- , and ClO_3^- have values of 0.6137, 0.6037, 0.4410, and 0.5533, respectively (Table 2). The lowest R^2 value is for ClPO_4^{3-} at 0.1705. The p-values for nearly all analytes are $\ll 0.001$, even with a Bonferroni Correction, with Cl⁻ having the only value above 0.05. The highest out-of-the-bag-box explained variance values from the random forest models are for total salts and KClO_3^{+} and Sr^{2+} at 75.62% and 63%, respectively for both analytes. The lowest explained variance is for Sr^{2+} at 37%. Values for NO_3^- , PO_4^{3-} , ClO_4^- , and N:P ratio and ClO_3^- are negative 52% and 48%, respectively. The explained variance for total salts is 45% and the variance for ClO_3^- is 43%. We also evaluated the most important and least important variables in the random forest models based on node purity. The most important variable for the majority of analytes is elevation, while distance from the glacier is most important for N:P ratio and latitude for ClO_3^- (Table 2). The least important variables are distance from the coast and latitude for every analyte, except ClO_3^- and NH_4^+ , for which distance from the glacier is least important.

5. Discussion

5.1. Implications for ecological habitat suitability

By establishing geochemical zones for the Shackleton Glacier region, we can better understand the relationship between geochemistry and geography, and ultimately biogeography. As stated in the introduction, we focused particularly on total water-soluble salt concentrations, water-soluble N:P ratios, and ClO_4^- and ClO_3^- concentrations.

5.1.1. Elevation and moisture controls on total water-soluble salt gradients

The elevational trends of total salt concentrations at the Shackleton Glacier are similar to those previously described in the TAM, where soils from higher elevation sites typically have higher salt concentrations (Bottos et al., 2020; Lyons et al., 2016; Magalhães et al., 2012). Our results are also consistent with those from Scarrow et al. (2014) who found that salt concentrations typically decreased with distance from the glacier in the Beardmore and Lennox King Glacier regions. Our

261 total water-soluble salt interpolation maps highlight the spatial variability in Shackleton Glacier region soils (Fig. 6). The
262 most spatially variable location is Robert Massif, which does not appear to follow local elevational, latitudinal, and/or
263 distance inland gradients. This heterogeneity is not necessarily due to currently active soil leaching, as the soil moisture
264 values are not drastically different between the samples (Table S2). Though the variability in cation concentrations is likely
265 due to weathering of tills, scree, and bedrock (Claridge and Campbell, 1968), recent work on the isotopic composition of
266 water-soluble nitrate and sulfate, the major anions in the upper zone, suggests a common, atmospheric source (Diaz et al.,
267 2020b).

268 We argue that the heterogeneity in the total salt concentrations at Roberts Massif (Figs. 2; 6) is probably related to
269 different and complex wetting history, where seasonal snow patch melt may pool in local depressions, transporting water-
270 soluble salts from slightly higher elevations and/or from saline wet-patches (Levy et al., 2012). This is demonstrated on a
271 larger scale at Thanksgiving Valley, a glacially carved valley, where the higher concentrations of salts in the center of the
272 valley are likely due to the transport of salts from nearby higher elevation slopes during melting events. This is further
273 evidenced by the presence of two small, closed-basin ponds in the center of the valley, which likely formed from glacial melt
274 and may have been larger in size in the recent past (Diaz et al., 2019). Similarly, streams and meltwater tracks in the MDV
275 leach soils and carry salts into closed basin, brackish to hyper-saline lakes, where salts are cryoconcentrated over time
276 (Lyons et al., 1998). Our results suggest that elevation and wetting history are important contributors to total salt gradients in
277 the Shackleton Glacier region, as they influence the accumulation of salts and subsequent leaching from soils.

278 5.1.2. Influence of glacial history on water-soluble N:P ratios

279 Stoichiometric dependencies have been identified for Antarctic terrestrial organisms, where nutrient concentrations,
280 in addition to soil aridity, limit ecosystem development (Nkem et al., 2006). Since nitrate is primarily derived from
281 atmospheric deposition and phosphorus is primarily liberated from minerals by chemical weathering in the CTAM, many
282 inland and higher elevation soils have accumulated high concentrations of NO_3^- , resulting in stoichiometric imbalance with
283 soluble PO_4^{3-} (Ball et al., 2018; Barrett et al., 2007; Diaz et al., 2020b; Lyons et al., 2016; Nkem et al., 2006). As in the
284 MDV, younger and coastal soils at lower elevations in the Shackleton Glacier region have the lowest water-soluble N:P
285 ratios, driven by relatively low concentrations of NO_3^- and high concentrations of PO_4^{3-} due to an increase in moisture
286 content and chemical weathering (Heindel et al., 2017) (Fig. 2; 4). It is not surprising that life was conspicuous in these soils,
287 with thick lichen growth on several rocks and the presence of both Collembola and mites at Mt. Speed and Mt. Wasko (Fig.
288 S1). However, despite overall elevational and latitudinal gradients, some inland locations in the middle and upper zones have
289 water-soluble N:P ratios near those from the lower zone (Fig. 2).

290 The interpolation model from Bennett Platform shows that some locations near the glacier have lower total water-
291 soluble salt concentrations (Fig. 6), similar to soils surveyed in the MDV (Bockheim, 2002). However, the samples near the
292 glacier at Bennett Platform not only have lower total salt concentrations, they also have lower N:P ratios than samples

293 collected further inland. This is also the case for the middle zone locations (Fig. 2f). We argue this is due to differences in
294 glacial history between the locations. Our previous work showed that soils near the glacier are younger than soils further
295 inland in the Shackleton Glacier region (Diaz et al., 2020a). These soils are shielded from nitrate accumulation during glacial
296 periods, and the recently exposed rocks likely serve as fresh mineral weathering material for PO_4^{3-} mobilization (Heindel et
297 al., 2017). Recently exposed and relatively nutrient rich soils might be important refugia for invertebrates. Previous
298 hypotheses have suggested that organisms may have persisted at higher elevations during glacial periods (Bennett et al.,
299 2016; Stevens and Hogg, 2003). However, abiotic gradients in the Beardmore Glacier region suggest that higher elevation
300 soils have salt concentrations that would classify them as unsuitable habitats (Lyons et al., 2016). If few organisms survived
301 glaciations, the near-glacier, relatively P-rich soils may be important in helping communities recover and restructure post-
302 glaciation.

303 5.1.3. High and variable ClO_4^- and ClO_3^- concentrations

304 Our ClO_4^- and ClO_3^- concentrations include the highest measured in Antarctica to date and are comparable to
305 concentrations from the Atacama and Mojave Deserts (Jackson et al., 2015). Though not a strong correlation, the highest
306 elevation samples (upper zone) have the highest ClO_4^- and ClO_3^- concentrations (Fig. 2g; 2j). Similar to NO_3^- , ClO_4^- and
307 ClO_3^- are derived from atmospheric deposition and because of their [high](#) solubilities, their accumulations are related to
308 wetting and glacial histories (Jackson et al., 2016, 2015). Therefore, soils which have been exposed for long periods of time
309 and have not experienced snow or ice melt, such as those from Schroeder Hill and Roberts Massif, are able to accumulate
310 high concentrations of ClO_4^- and ClO_3^- . Interestingly, our ClO_4^- concentrations are lower (maximum of $\sim 1.9 \text{ g L}^{-1}$) than the
311 highest recorded tolerance (1.1 M ($\sim 130 \text{ g L}^{-1}$) NaClO_4) for the extremotolerant bacteria *Planococcus halocryophilus*, yet a
312 recent study shows no detectable biomass for Schroeder Hill samples (Dragone et al., 2020). (Per)chlorates are strong
313 oxidizers and are well established as toxic, thus the concentrations of ClO_4^- and ClO_3^- might be additional, crucial indicators
314 of habitat suitability. However, the concentrations are highly heterogeneous across our sampled locations (Fig. 2k-l), and
315 unlike ClO_3^- , neither the multiple linear regression nor random forest models were able to adequately capture the variability
316 in ClO_4^- concentrations (Table 2).

317 5.2. Machine learning as a tool to predict soil geochemical trends

318 We sought to evaluate our multiple linear regression and random forest models using a testing dataset from the
319 Shackleton Glacier region ($n = 31$) and a second dataset from the Darwin Mountains ($\sim 80^\circ\text{S}$) ($n = 10$) (Magalhães et al.,
320 2012). Few published/available TAM dataset include sample GPS coordinates, soil moisture, and water-soluble ion
321 geochemistry. As stated in Section 3.3, the Shackleton Glacier region test data were not included in the random forest model
322 generation so we could evaluate our models with an independent dataset. For the Darwin dataset, distance from the glacier,
323 distance from the coast, and elevation were determined using the Reference Elevation Model of Antarctica (REMA), while
324 location, soil moisture and geochemistry were retrieved from the literature (Howat et al., 2019; Magalhães et al., 2012). We

325 evaluated all 15 analytes from the original models with the Shackleton dataset and, due to a lack of data, only evaluated 7
326 analytes from the Darwin soils (Figure 7).

327 Both the multiple linear regression and random forest model outputs are moderately well-correlated for the
328 Shackleton dataset, as determined by Pearson correlations between the measured and predicted values (Fig. 7a; Table 3). The
329 random forest models outperform the linear regression models for nearly every analyte, with the notable exceptions of FSr^{2+} ,
330 Na^+ , NH_3 , and PNO_3^{3-} , and nearly all p-values are <0.001 . For Cl^- , in particular, the random forest model significantly
331 outperforms the multiple linear regression model, with R^2 values of 0.67 and 0.16, respectively. Mg^{2+} :N:P molar ratio is the
332 most accurately predicted analyte, with R^2 values of 0.8879 and 0.5952 for the random forest and linear regression models,
333 respectively. However, the highest R^2 value for the multiple linear regression model is for Na^+ at 0.64 (Fig. 7a Table 3). In
334 terms of our analytes of interest regarding habitat suitability, total salts have the second strongest correlation (following N:P
335 ratio) in with the random forest model ($R^2 = 0.8154$), followed by water-soluble N:P ratio ($R^2 = 0.42$), ClO_4^- ($R^2 = 0.4078$),
336 and ClO_3^- ($R^2 = 0.7428$). N:P ratio in particular performs significantly better than the linear regression model ($R^2 = 0.05$).
337 Mean absolute error (MAE) and root mean squared error (RMSE) values indicate that the random forest models also have a
338 smaller error compared to the multiple linear regression models (Table 4). MAE values are lower than RMSE values for both
339 models, indicating the strong presence-influence of outliers in the testing dataset. This is unsurprising as the standard
340 deviation and coefficient of variation values for the entire dataset are relatively large for all analytes. Additionally, the strong
341 presence of outliers is likely one reason why the random forest models are stronger than the multiple linear regression
342 models.

343 Similar to the model performance in the Shackleton Glacier region, the water-soluble ion predictions for the Darwin
344 Glacier region are more strongly correlated with measured values in the random forest models compared to the multiple
345 linear regressions (Fig. 7b). In fact, the linear regression models fail for nearly all the Darwin samples and almost
346 concentration outputs are negative, which is likely due to overfitting during model generation. Here, Ca^{2+} and K^+ are
347 exceptions and the multiple linear regression models outperform the random forest models in both cases. MAE and RSME
348 values for both models are much higher than those for the Shackleton dataset (Table 4). On the other hand, the random forest
349 models perform particularly well for some analytes. Though a small sample size, the R^2 values for Mg^{2+} :N:P molar ratio and
350 KCa^{2+} are 0.68 and 0.66, respectively, with p-values $\ll 0.001$. Total salts is moderately correlated ($R^2 = 0.474$) and N:P
351 ratio has an R^2 value of 0.01, indicating poor model performance. It is unclear why Mg^{2+} and K^+ some analytes, such as N:P
352 molar ratio, are the most accurately predicted, though we suspect that this is due to 1) weathering trends of local lithology
353 across the TAM, since chemical weathering is probably the major source of these ions, and 2) deposition and accumulation
354 of atmospherically-derived ions at higher elevations (Diaz et al., 2020b).

355 It should be noted that the R^2 values simply measure the strength of the correlations between the measured and
356 predicted values. We performed slope tests by fitting bivariate lines using the standardized major axis (SMA) to further

357 understand the relationship between the two values using the `smatr` library in R (Warton et al., 2012). For this test, we
358 specifically evaluated the null hypothesis (H_0) where slope = 1, which would indicate whether an ideal, direct 1:1
359 relationship exists between the measured and predicted values. Test statistic values (t) were used to measure the sample
360 correlation between the residuals and fitted values (Warton et al., 2012). Test statistic values near 1 indicate that we reject
361 the null hypothesis. In other words, higher absolute test statistic values indicate a slope other than 1. Of the 15 analytes in the
362 Shackleton dataset, 57 analytes have slopes near 1 for the multiple linear regression models and 116 for the random forest, as
363 indicated by test statistic values less than 0.5. For the Darwin, ~~only one analyte, NO_3^- , has no analytes have a~~ test statistic
364 values less than 0.5 (Fig. 7; Table 3).

365 These data indicate that while some analytes have high correlations between measured and predicted values, the
366 models perform best with the Shackleton Glacier region soils. Additionally, though the relationship may not be 1:1, the
367 random forest models are effective at predicting the measured geochemical gradients. For example, similar to our data, the
368 Darwin Glacier samples generally have greater water-soluble N:P ratios and total water-soluble salt concentrations further
369 from the glacier and at higher elevations (Magalhães et al., 2012), a trend that is reflected by our model results despite offset
370 values. Additionally, corrections for the offset of the model from a slope = 1 (i.e. multiplying the model output value by the
371 regression slope) can be made to better estimate specific concentrations, though the difference between modeled and
372 measured values can still be up to 2x greater. Our sample size for building the multiple linear regression and random forest
373 models is small. We anticipate that, as more data are collected throughout the CTAM, these data can be added to the model
374 training dataset, expanding our prediction capabilities and increasing model reliability.

375 6. Conclusions

376 The soil ecosystems found in the Transantarctic Mountains are among the least diverse on Earth and their structure
377 is influenced by environmental ~~factors~~ variables. We characterized environmental and geochemical gradients in the
378 Shackleton Glacier region, which aid in our understanding of the abiotic properties in soils governing biodiversity and
379 biogeography. The 220 samples we analyzed represent a wide range of soil environments: those with different elevation,
380 latitude, longitude, glacial history, and geochemistry. We determined three soil zones: an upper zone near the head of the
381 glacier which is characterized by high total water-soluble salt concentrations, high water-soluble N:P ratios, and high ClO_4^-
382 and ClO_3^- concentrations, a lower zone with low total salt concentrations and higher PO_4^{3-} concentrations, and a middle zone
383 with intermediate values. The zones help elucidate the geographic influences on soil geochemistry. In addition, our total
384 water-soluble salt interpolations at Roberts Massif, Bennett Platform, and Thanksgiving Valley reflect the local small-scale
385 variability of salt concentrations and possible influences from soil age and wetting history.

386 Similar to previous studies, our results suggest that high elevation and inland soils, such as those from the upper
387 zone, were likely unsuitable candidates for refugia during the Last Glacial Maximum. However, glacial advance and retreat
388 and climate shifts may leach soils, lowering otherwise toxic total water-soluble salt concentrations and N:P ratios. These

389 more recently exposed soils may be particularly important in maintaining and reviving contemporary and past biological
390 communities.

391 Five geographic variables (latitude, longitude, elevation, distance from the coast, and distance from the glacier) and
392 soil moisture were correlated with soil geochemistry. We used these variables to develop multiple linear regression and
393 random forest models to predict ion concentrations and geochemical gradients. The model results generally reflected the
394 measured geochemical variability across the region. Test datasets from the Shackleton and Darwin Glacier regions showed
395 that the random forest models typically outperformed the multiple linear regression models when correlating measured and
396 predicted values, especially for the Darwin region. Though most correlations did not exhibit a 1:1 relationship and had
397 varying slopes, the random forest models were able to adequately predict geochemical gradients, as demonstrated by
398 moderate to high R^2 values between measured and model predicted concentrations. As terrestrial Antarctic geochemical
399 databases expand and are included in the random forest model training dataset, we anticipate the model's predictive
400 capabilities will expand and improve as well. While these results are currently most applicable for Central Transantarctic
401 Mountain soils, similar techniques can be applied to other hyper-arid environments (e.g. Namib and Atacama Deserts, Mars)
402 to inform patterns of biodiversity and biogeography.

403 **Author Contributions**

404 The project was designed and funded by BJA, DHW, IDH, NF, and WBL. Fieldwork was conducted by BJA, DHW, IDH,
405 NF, and MAD. CBG, SAW, and MAD prepared and analyzed the samples for water-soluble ion and nutrient analyses. WAJ
406 prepared and analyzed the samples for ClO_4^- and ClO_3^- . MAD generated the scripts and performed the analyses for the IDW
407 interpolations, multiple linear regression, and random forest models. MAD wrote the article with contributions and edits
408 from all authors.

409 **Data Availability Statement**

410 The datasets generated for this study are included in the article or supplementary materials.

411 **Competing Interests**

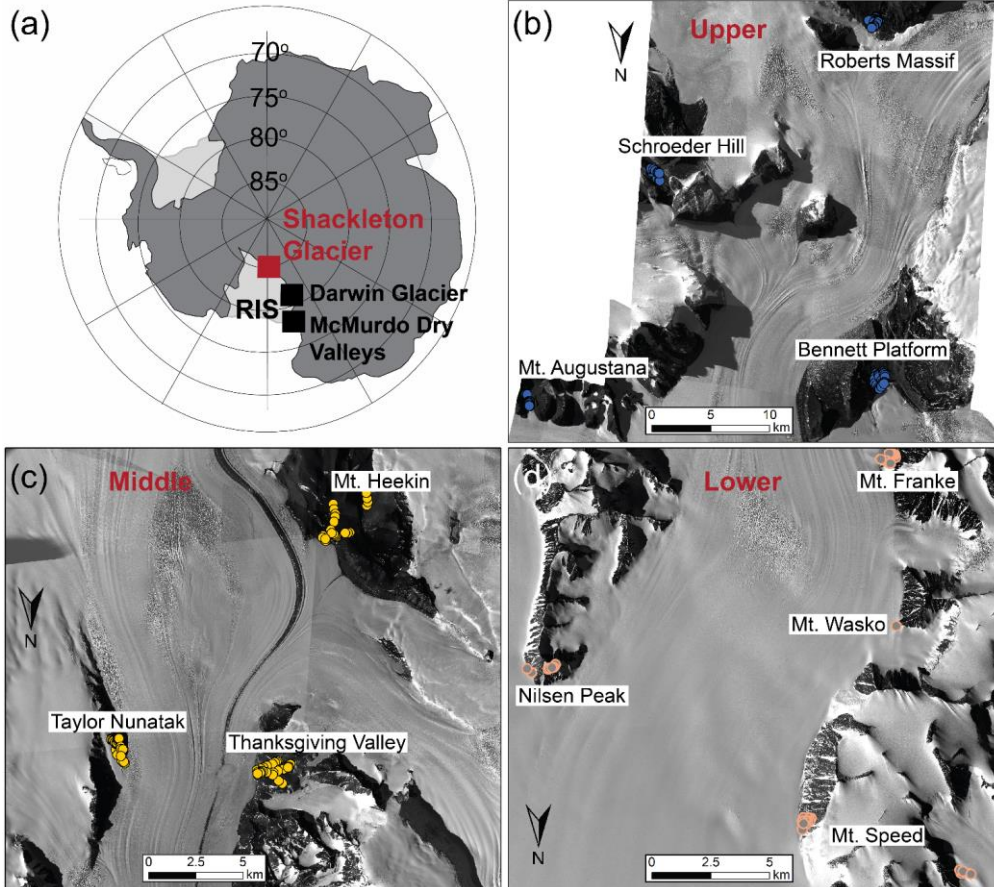
412 The authors declare that they have no conflict of interest.

413 **Acknowledgments**

414 We thank the United States Antarctic Program (USAP), Antarctic Science Contractors (ASC), Petroleum Helicopters Inc.
415 (PHI), and Marci Shaver-Adams for logistical and field support. Additionally, we thank Daniel Gilbert for help with initial
416 laboratory analyses at The Ohio State University. [We are grateful to Dr. Peter Convey and Dr. Natasja van Gestel for](#)
417 [thoughtful reviews which strengthened our results and broader implications.](#) This work was supported by NSF OPP grants
418 1341631 (WBL), 1341618 (DHW), 1341629 (NF), 1341736 (BJA), and NSF GRFP fellowship 60041697 (MAD).
419 Geospatial support for this work provided by the Polar Geospatial Center under NSF OPP grants 1043681 and 1559691.

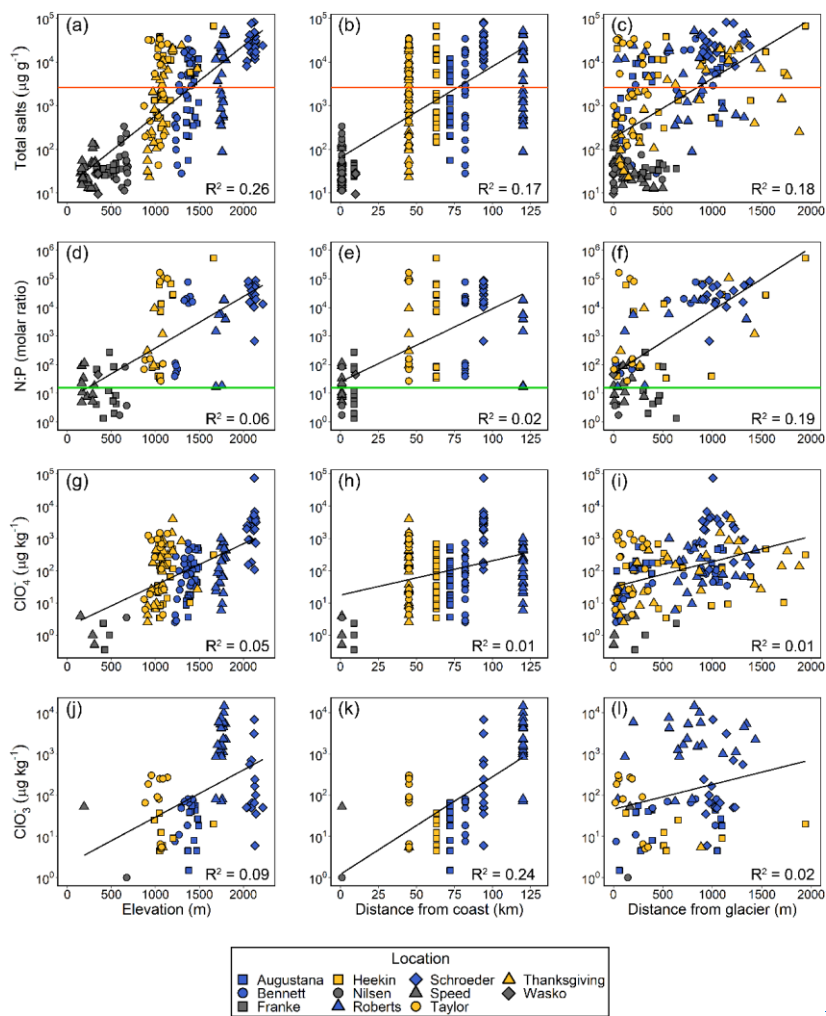
420

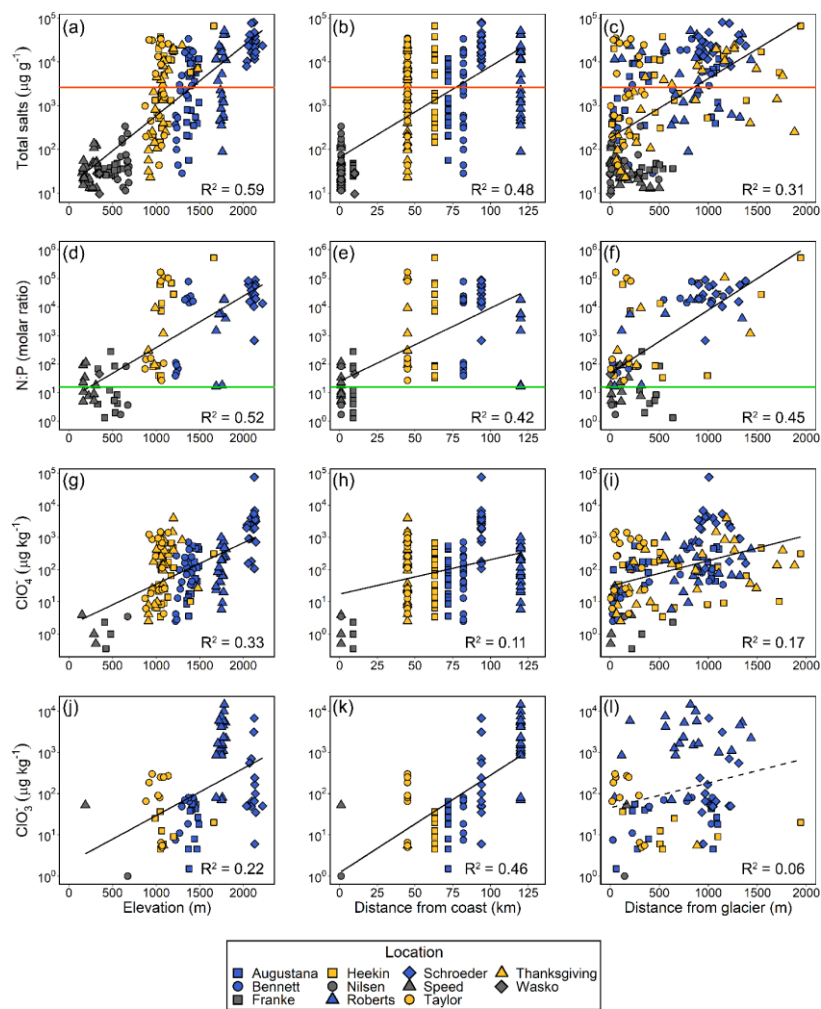
421 Figures



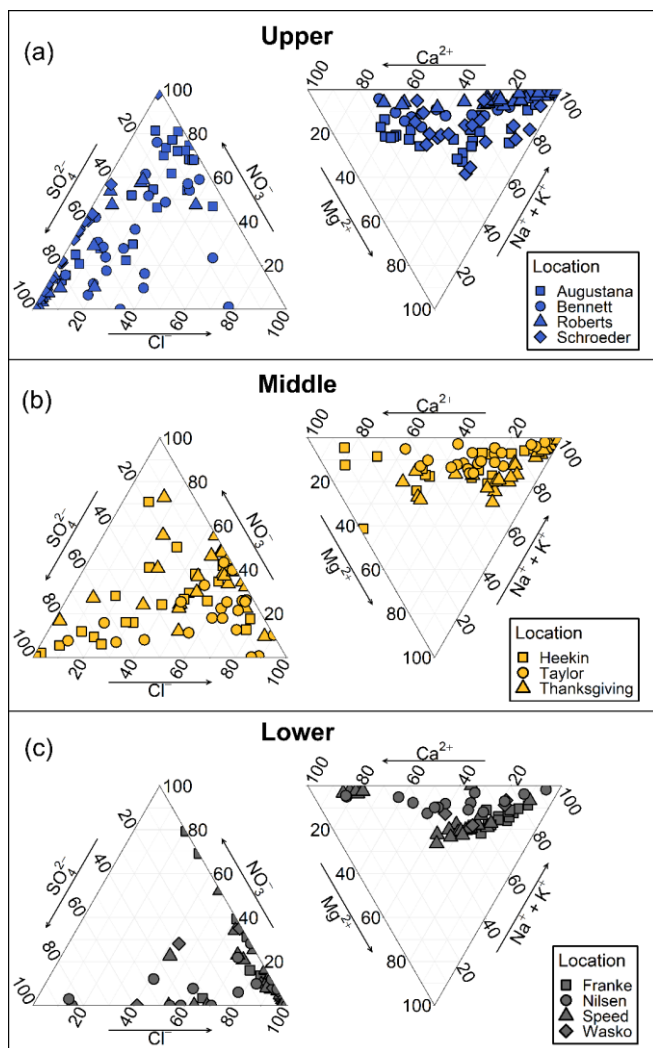
422

423 Figure 1. Samples were collected and analyzed from the exposed soils along the Shackleton Glacier, a major outlet glacier of
424 the EAIS (a), in three zones. The upper zone (b) was located at the head of Shackleton Glacier, the middle zone (c) was the
425 central portion, and the lower zone (d) was at the mouth of the glacier where it drains into the Ross Sea. Satellite images
426 were provided courtesy of the Polar Geospatial Center (PGC).
427

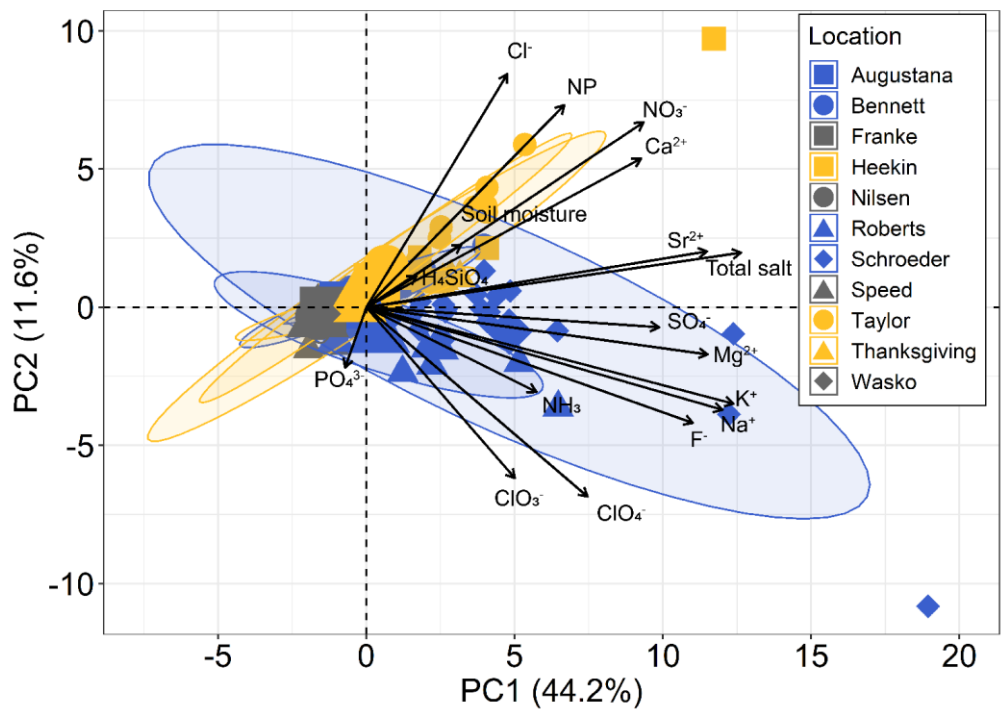




430 Figure 2. Total water-soluble salts, water-soluble N:P molar ratio, and ClO_4^- and ClO_3^- concentrations (log scale) were
431 compared to elevation, distance from the coast, and distance from the glacier for samples from the three geographic zones
432 (blue for upper, yellow for middle, grey for lower zones). Linear regression lines are plotted, where dashed lines represent
433 regressions where $p > 0.05$ with a Bonferroni Correction, and R^2 values are reported for each relationship. The horizontal
434 orange line represents nematode salt tolerance of ~2,600 (Nkem et al., 2006) and the green line represents the Redfield
435 ratio, N:P = 16 for phytoplankton in the ocean.
436



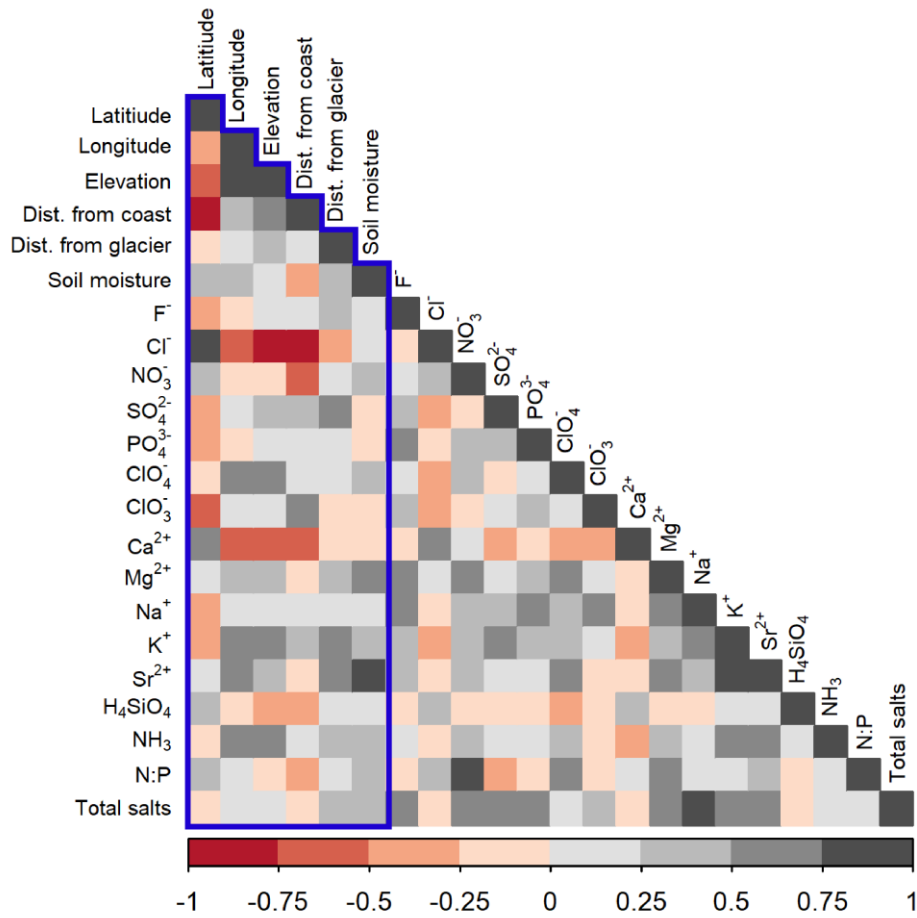
437
 438 Figure 3. Anion and cation ternary diagrams for the three geographic zones.
 439



440

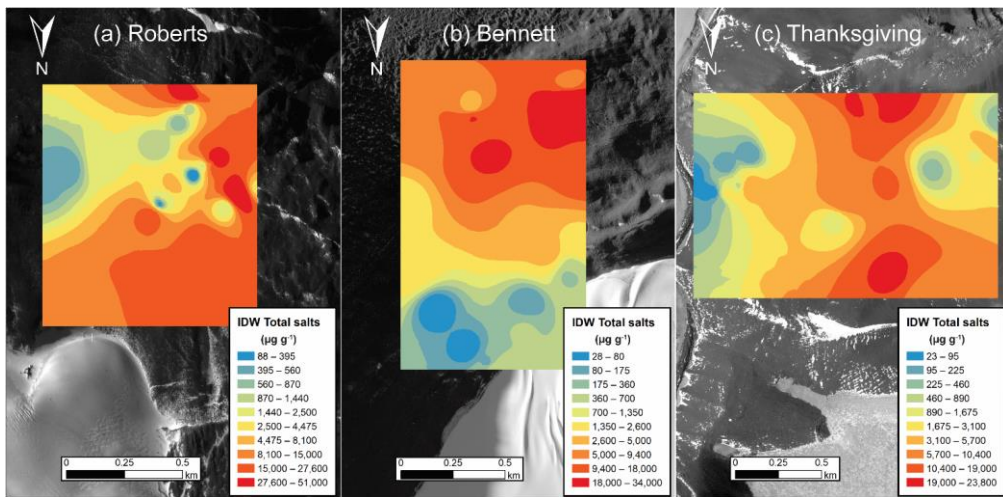
441 Figure 4. Principal component analysis (PCA) biplot generated in R using factoextra and built in R software libraries with all
 442 anions, cations, nutrients, and soil moisture for the three geographic zones. [The PCA is based on the correlation matrix \(i.e.](#)
 443 [scale = TRUE](#)). Principal component 1 and principal component 2 are plotted on the x and y axes, respectively. Shaded
 444 ellipses represent 95% confidence intervals.

445

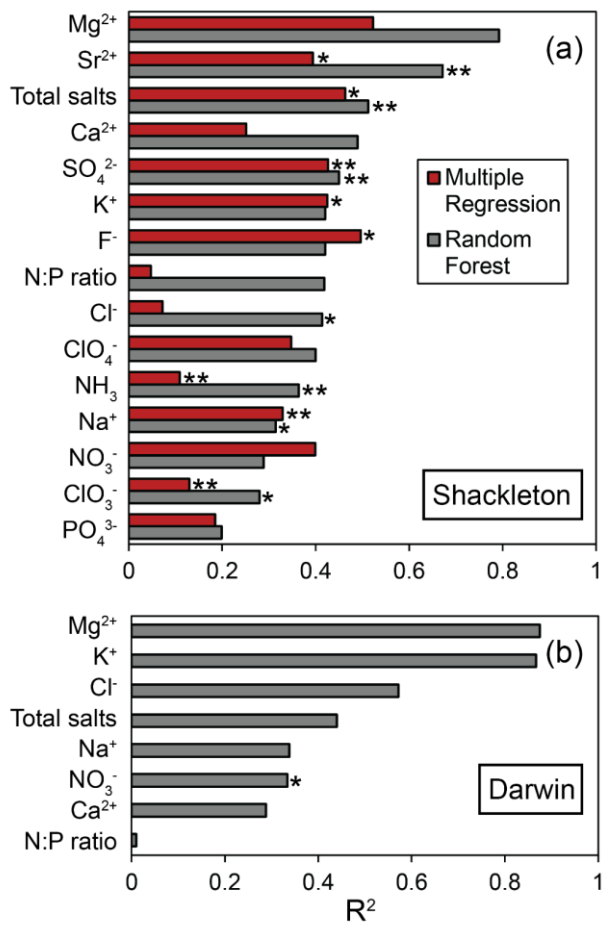


447

448 Figure 5. Spearman's rank correlation matrix generated in R using the corrplot library. The colors represent correlation
 449 coefficients, indicating the strength and magnitude of the correlation. The blue box indicates the geographic variables and
 450 soil moisture, which were variables used in the multiple linear regression and random forest models. [Familywise type I error](#)
 451 [corrections were not applied for this analysis.](#)
 452



453
 454 Figure 6. Inverse distance weighted (IDW) interpolations of total salt concentration for Roberts Massif (a), Bennett
 455 Platform (b), and Thanksgiving Valley (c). The color scale represents the 10 natural breaks in the data. Interpolations were created and
 456 mapped using the Geostatistical Analyst tool in ArcMap 10.3.
 457



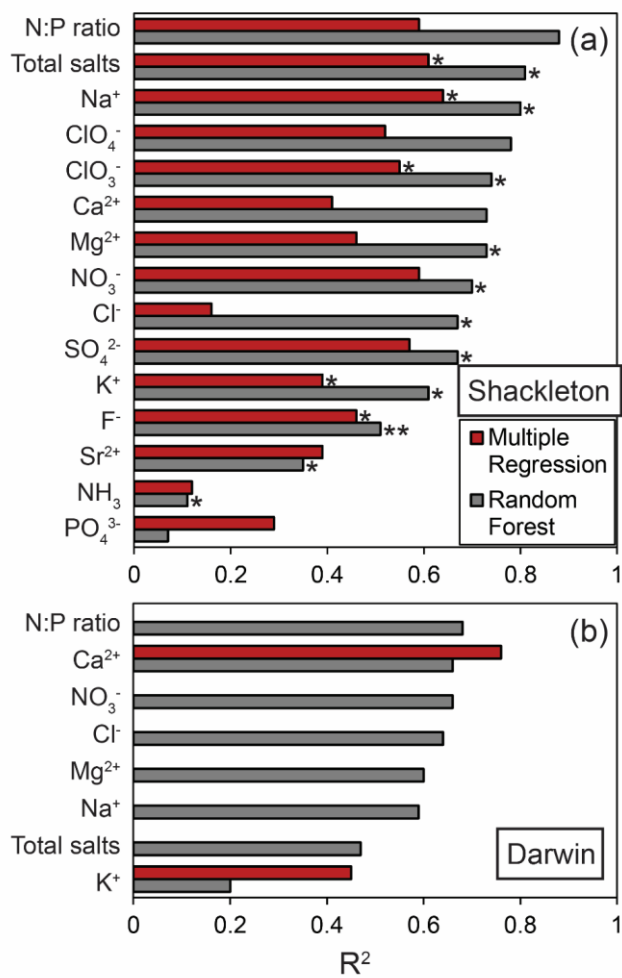


Figure 7. R² values for the multiple linear regression and random forest model predicted and measured values for the different analytes (Table 3). Test datasets include the Shackleton Glacier region (n = 31) and the Darwin Glacier region (n = 10) (Magalhães et al., 2012). Analytes with slopes near 1, indicating good agreement between measured and predicted values, are indicated (* t < 0.5; ** t < 0.20).

465
466

Table 1. Overview of geography, soil moisture, and water-soluble ions from the Shackleton Glacier region. The minimum values reported are those within the detection limits. Individual sample concentrations are detailed in Table S2.

	Max	Min	Mean	STD	CV
Elevation (m)	2,220	150	1,130	551	48
Distance from coast (km)	120	1	55	38	68
Distance from glacier (m)	1,940	1	519	472	90
Soil moisture (%)	12.3	0.1	2.1	2.1	102
F ⁻ (μg g ⁻¹)	120	0.39	8.87	11.78	133
Cl ⁻ (μg g ⁻¹)	13,600	1.59	615	1,780	289
NO ₃ ⁻ (μg g ⁻¹)	38,400	0.10	1,470	3,450	235
SO ₄ ²⁻ (μg g ⁻¹)	55,300	0.08	4,390	8,080	184
PO ₄ ³⁻ (μg kg ⁻¹)	4,200	76.09	381	560	147
ClO ₄ ⁻ (μg kg ⁻¹)	75,000	0.35	985	6,020	611
ClO ₃ ⁻ (μg kg ⁻¹)	14,500	1.00	1,170	2,500	214
Ca ²⁺ (μg g ⁻¹)	4,400	0.55	839	1,160	139
Mg ²⁺ (μg g ⁻¹)	6,280	0.12	293	705	240
Na ⁺ (μg g ⁻¹)	25,300	0.39	1,140	2,880	252
K ⁺ (μg g ⁻¹)	440	0.86	28.31	51.61	182
Sr ²⁺ (μg g ⁻¹)	46.61	0.01	8.63	10.31	119
H ₄ SiO ₄ (μg g ⁻¹)	60.78	1.14	21.78	11.03	50.67
NH ₃ (μg kg ⁻¹)	5,080	18.85	324	587	181
N:P ratio (molar)	526,000	0.29	23,600	62,700	266
Total salt (μg g ⁻¹)	80,500	9.46	7,932	13,300	167

STD, standard deviation; CV, coefficient of variation

467

Table 2. Out-of-the-bag multiple linear regression and random forest model statistics generated in R. [All geochemical data were log-transformed.](#)

	Multiple regression		Random forest		
	R ²	p-value	Variance explained (%)	Most important variable	Least important variable
F	0.2747	<<0.001	5736	Elevation	Distance from coast
Cl ⁻	0.0519	<<0.001	2060	Elevation	Distance from east Longitude
NO ₃ ⁻	0.1852	<<0.001	-460	Distance from glacier Elevation	Distance from east Longitude
SO ₄ ²⁻	0.3753	<<0.001	4462	Elevation	Distance from east Longitude
PO ₄ ³⁻	0.176	<<0.001	-74	Latitude Elevation	Distance from coast
ClO ₄ ⁻	0.441	<<0.001	-348	Elevation	Distance from coast
ClO ₃ ⁻	0.5533	<<0.001	4363	Latitude	Distance from glacier
Ca ²⁺	0.2644	<<0.001	4660	Soil moisture Elevation	Distance from coast
Mg ²⁺	0.2949	<<0.001	2261	Elevation	Distance from east Longitude
Na ⁺	0.2165	<<0.001	3875	Elevation	Distance from east Longitude
K ⁺	0.4048	<<0.001	6260	Elevation	Distance from coast
Sr ²⁺	0.5534	<<0.001	6237	Elevation	Distance from coast
NH ₃	0.29	<<0.001	5438	Elevation	Distance from glacier coast
N:P	0.3760	<<0.001	-352	Distance from glacier	Distance from east Longitude
Total salts	0.3761	<<0.001	4575	Elevation	Distance from east Longitude

472
473
474
475
476

Table 3. Multiple linear regression and random forest statistics between predicted and measured concentrations from the Shackleton and Darwin Glacier regions. R² and p-values are reported for the correlations between measured and predicted concentrations. Regression slopes and test statistic values (t) were calculated using the smatr library (Warton et al., 2012) in R to evaluate the null hypothesis (H₀) of slope = 1. Higher test statistic values (closer to one) indicate that we reject the null hypothesis. [All geochemical data were log-transformed.](#)

Analyte	Multiple Linear Regression				Random Forest			
	R ²	p-value	Reg. slope	Test statistic (t) for H ₀ slope = 1	R ²	p-value	Reg. slope	Test statistic (t) for H ₀ slope = 1
Shackleton								
<u>N:P ratio</u> _{Mg³}	0.590.5 2	<<0.001<<0.001	0.580.5 2	-0.720-0.711	0.880.7 9	<<0.001<<0.001	0.640.5 8	-0.7920-780
Total salts	0.610.3 9	<<0.001<<0.001	0.714.2 2	0.483*0.247*	0.810.6 7	<<0.001<<0.001	0.860.9 1	-0.324* 0.166**
<u>Na⁺Total salts</u>	0.640.4 6	<<0.001<<0.001	0.760.7 6	-0.424* 0.343*	0.800.5 1	<<0.001<<0.001	0.890.9 3	-0.262* 0.107**
<u>ClO₂⁻ Ca²⁺</u>	0.520.2 5	<<0.0010.004	0.600.4 2	-0.614-0.747	0.780.4 9	<<0.001<<0.001	0.710.6 1	-0.590-0.586
<u>ClO₂⁻ SO₄²⁻</u>	0.550.4 3	0.009<<0.001	0.721.0 7	- 0.454*0.093*	0.740.4 5	<0.001<<0.001	0.861.1 0	- 0.284*0.130*
<u>Mg²⁺K⁻</u>	0.460.4 2	<<0.001<<0.001	0.631.5 4	-0.5500-504*	0.730.4 2	<<0.001<<0.001	0.761.7 9	-0.469*0.629
<u>Ca²⁺F⁻</u>	0.410.5 0	<<0.001<<0.001	0.574.2 2	-0.6130-267*	0.730.4 2	<<0.001<<0.001	0.741.7 8	-0.5120-617
<u>NO₃:N:P ratio</u>	0.590.0 5	<<0.0010.241	0.620.5 9	-0.615-0.517	0.700.4 2	<<0.001<<0.001	0.750.3 5	-0.465* 0.867
<u>Sr²⁺Cl⁻</u>	0.350.0 7	0.0260.144	0.540.2 8	-0.631-0.867	0.670.4 1	<0.001<<0.001	0.820.7 0	-0.326* 0.424*
<u>SO₄²⁻ ClO₂⁻</u>	0.570.3 5	<<0.001<<0.001	0.632.0 1	-0.5840-685	0.670.4 0	<<0.001<<0.001	0.833.4 0	-0.310*0.897
<u>Cl⁻NH₃</u>	0.160.1 1	0.0280.070	0.381.0 4	- 0.7730.037**	0.670.3 6	<<0.001<<0.001	0.761.0 9	- 0.428*0.106*
<u>K⁺Na⁺</u>	0.390.3 3	<<0.001<<0.001	0.690.9 1	-0.429* 0.112**	0.610.3 1	<<0.0010.001	0.831.5 4	- 0.291*0.473*
<u>FNO₃⁻</u>	0.460.4 0	<<0.001<<0.001	0.760.4 7	-0.352* 0.725	0.510.2 9	<<0.0010.002	0.910.5 6	-0.141** 0.594
<u>NH₃ClO₂</u>	0.120.1 3	0.0520.043	0.574.2 0	- 0.5280.197**	0.110.2 8	0.0680.002	0.610.7 1	-0.475* 0.382*
<u>PO₄³⁻ PO₄³⁻</u>	0.290.1 8	0.0700.016	0.320.5 0	-0.857-0.645	0.070.2 0	0.4080.022	0.380.1 5	-0.764-0.967
Darwin								
<u>N:P ratio</u> _{Mg³}	-	-	-	-	0.680.8 7	0.021<<0.001	0.540.3 9	-0.765-0.948

Formatted

Formatted

Formatted

Formatted Table

Formatted

Formatted

Formatted

Formatted

Formatted

Formatted

Formatted

Formatted

Formatted

Formatted

Formatted

Formatted

Formatted

Formatted

Formatted

Formatted

Formatted

Formatted

Formatted

Formatted

Formatted

Formatted

Formatted

Formatted

Formatted

Formatted

Formatted

Formatted

Formatted

Formatted

Formatted

Formatted

Formatted

Formatted

Formatted

Formatted

Formatted

Formatted

Formatted

Formatted

Formatted

Formatted

Ca ²⁺ K ⁺	0.76-	0.001-	0.66-	-0.645-	0.660.8 7	0.004<<0.001	0.500.4 9	-0.785-0.895
NO ₃ Cl	-	-	-	-	0.660.5 7	0.0040.011	0.490.1 3	-0.794-0.984
Cl Total salts	-	-	-	-	0.640.4 4	0.0050.001	0.223.2 5	-0.9620.940
Mg ²⁺ Na ⁺	-	-	-	-	0.600.3 4	0.1400.078	0.670.2 3	-0.544-0.931
Na ⁺ NO ₃ ⁻	-	-	-	-	0.590.3 3	0.1600.080	0.420.6 5	-0.836- 0.476*
Total saltsCa ²⁺	-	-	-	-	0.470.2 9	0.0280.110	0.420.1 7	-0.802-0.961
K ⁺ N:P ratio	0.45-	0.070-	0.62-	-0.550-	0.200.0 1	0.2670.765	0.288.0 4	-0.8820.970

* t < 0.5; ** t < 0.20

Formatted

Formatted

Formatted

Formatted

Formatted

Formatted

Formatted

Formatted

Formatted

Formatted

Formatted

Formatted

Formatted

Formatted

Formatted

Formatted

Formatted

Formatted

Formatted

Formatted

Formatted

Formatted

Formatted

Formatted

Formatted

Formatted

Formatted

Formatted

Formatted

Formatted

Formatted

Formatted

Formatted

Formatted

Formatted

Formatted

Formatted

Formatted

Formatted

Formatted

Formatted

Formatted

Formatted

Formatted

Formatted

Formatted

Formatted

478
479

Table 4. Multiple linear regression and random forest model mean absolute error (MAE) and root mean squared error (RMSE). All geochemical data were log-transformed for the analysis.

Analyte	Multiple Linear Regression		Random Forest	
	MAE	RMSE	MAE	RMSE
Shackleton				
N:P ratio	2.19300	2.73461	1.75204	2.11347
Total salts	1.453.74	1.694.96	0.861.83	1.172.90
Na ⁺ Total salts	1.235.640	1.527.070	0.834.400	1.137.030
ClO ₄ ⁻ Ca ²⁺	1.33797	1.621.100	0.91554	1.12912
ClO ₃ ⁻ SO ₄ ²⁻	1.073.310	1.673.890	1.012.200	1.263.780
Mg ²⁺ K ⁺	1.7815.86	2.0821.16	1.0713.48	1.4825.61
Ca ²⁺ F ⁻	1.843.14	2.214.19	1.183.13	1.536.31
NO ₃ ⁻ N:P ratio	1.9639.700	2.2959.300	1.567.310	1.9317.210
Sr ²⁺ Cl ⁻	1.05936	1.171.540	0.59658	0.821.240
SO ₄ ²⁻ ClO ₄ ⁻	1.581.180	1.941.560	1.35875	1.672.960
ClNH ₃	2.11214	2.39301	1.07158	1.5244
K ⁺ Na ⁺	0.73883	0.891.170	0.56918	0.721.730
FNO ₃ ⁻	0.481.200	0.61.910	0.461.130	0.582.040
NH ₃ ClO ₃ ⁻	0.671.110	0.831.630	0.65343	0.861.050
PO ₄ ³⁻ PO ₄ ²⁻	0.75428	0.96690	0.78261	1.14742
Darwin				
N:P ratio	2676.300	2676.320	1.48302	1.73475
Ca ²⁺ K ⁺	5.791.060	5.851.060	2.6313.33	2.8315.84
NO ₃ ⁻ Cl ⁻	261206.000	261206.000	3.192.140	3.523.330
Cl ⁻ Total salts	372215.000	372215.000	2.995.540	3.327.590
Mg ²⁺ Na ⁺	4608.330	4608.530	2.891.500	3.062.600
Na ⁺ NO ₃ ⁻	245128.000	245128.000	2.573.260	2.884.870
Total salts	13970.300	13970.300	1.221.410	1.672.070
K ⁺ N:P ratio	30.818.100.000	30.818.100.000	1.0018.700	1.1946.900

MAE, mean absolute error; RMSE, root mean squared error

Formatted Table

Formatted Table

480

481 **References**

- 482 Antipov, E. A. and Pokryshevskaya, E. B.: Mass appraisal of residential apartments: An application of Random forest for
483 valuation and a CART-based approach for model diagnostics, *Expert Syst. Appl.*, 39(2), 1772–1778,
484 doi:10.1016/j.eswa.2011.08.077, 2012.
- 485 Ball, B. A., Adams, B. J., Barrett, J. E., Wall, D. H. and Virginia, R. A.: Soil biological responses to C, N and P fertilization
486 in a polar desert of Antarctica, *Soil Biol. Biochem.*, 122, 7–18, doi:10.1016/J.SOILBIO.2018.03.025, 2018.
- 487 Balter-Kennedy, A., Bromley, G., Balco, G., Thomas, H. and Jackson, M. S.: A 14.5-million-year record of East Antarctic
488 Ice Sheet fluctuations from the central Transantarctic Mountains, constrained with cosmogenic ³He, ¹⁰Be, ²¹Ne, and ²⁶Al,
489 *Cryosph.*, 14(8), 2647–2672, doi:10.5194/tc-2020-57, 2020.
- 490 Barrett, J. E., Virginia, R. A., Wall, D. H., Cary, S. C., Adams, B. J., Hacker, A. L. and Aislabie, J. M.: Co-variation in soil
491 biodiversity and biogeochemistry in northern and southern Victoria Land, Antarctica, *Antarct. Sci.*, 18(4), 535–548,
492 doi:10.1017/S0954102006000587, 2006.
- 493 Barrett, J. E., Virginia, R. A., Lyons, W. B., McKnight, D. M., Prisco, J. C., Doran, P. T., Fountain, A. G., Wall, D. H. and
494 Moorhead, D. L.: Biogeochemical stoichiometry of Antarctic Dry Valley ecosystems, *J. Geophys. Res.*, 112(G1), G01010,
495 doi:10.1029/2005JG000141, 2007.
- 496 Beet, C. R., Hogg, I. D., Collins, G. E., Cowan, D. A., Wall, D. H., Adams, B. J., Beet, C., Hogg, I., Collins, G., Cowan, D.
497 and Adams, B.: Genetic diversity among populations of Antarctic springtails (Collembola) within the Mackay Glacier
498 ecotone 1, *Genome*, 59, 762–770, doi:10.1139/gen-2015-0194, 2016.
- 499 Bennett, K. R., Hogg, I. D., Adams, B. J. and Hebert, P. D. N.: High levels of intraspecific genetic divergences revealed for
500 Antarctic springtails: evidence for small-scale isolation during Pleistocene glaciation, *Biol. J. Linn. Soc.*, 119(1), 166–178,
501 doi:10.1111/bij.12796, 2016.
- 502 Bockheim, J. G.: Landform and Soil Development in the McMurdo Dry Valleys, Antarctica: A Regional Synthesis, *Arctic*,
503 *Antarct. Alp. Res.*, 34(3), 308–317, doi:10.1080/15230430.2002.12003499, 2002.
- 504 Bockheim, J. G.: Functional diversity of soils along environmental gradients in the Ross Sea region, Antarctica, *Geoderma*,
505 144(1–2), 32–42, doi:10.1016/j.geoderma.2007.10.014, 2008.
- 506 Bottos, E. M., Laughlin, D. C., Herbold, C. W., Lee, C. K., McDonald, I. R. and Cary, S. C.: Abiotic factors influence
507 patterns of bacterial diversity and community composition in the Dry Valleys of Antarctica, *FEMS Microbiol. Ecol.*, 96(5),
508 42, doi:10.1093/femsec/fiaa042, 2020.
- 509 Breiman, L.: Random forests, *Mach. Learn.*, 45(1), 5–32, doi:10.1023/A:1010933404324, 2001.
- 510 Caruso, T., Hogg, I. D., Nielsen, U. N., Bottos, E. M., Lee, C. K., Hopkins, D. W., Cary, S. C., Barrett, J. E., Green, T. G.
511 A., Storey, B. C., Wall, D. H. and Adams, B. J.: Nematodes in a polar desert reveal the relative role of biotic interactions in
512 the coexistence of soil animals, *Commun. Biol.*, 2(63), doi:10.1038/s42003-018-0260-y, 2019.
- 513 Claridge, G. G. C. and Campbell, I. B.: Soils of the Shackleton glacier region, Queen Maud Range, Antarctica, *New Zeal. J.*
514 *Sci.*, 11(2), 171–218, 1968.
- 515 Collins, G. E., Hogg, I. D., Convey, P., Barnes, A. D. and McDonald, I. R.: Spatial and temporal scales matter when
516 assessing the species and genetic diversity of springtails (Collembola) in Antarctica, *Front. Ecol. Evol.*, 7, 76,
517 doi:10.3389/fevo.2019.00076, 2019.
- 518 Collins, G. E., Hogg, I. D., Convey, P., Sancho, L. G., Cowan, D. A., Lyons, W. B., Adams, B. J., Wall, D. H. and Green, T.
519 G. A.: Genetic diversity of soil invertebrates corroborates timing estimates for past collapses of the West Antarctic Ice Sheet,
520 *Proc. Natl. Acad. Sci. U. S. A.*, 117(36), 22293–22302, doi:10.1073/pnas.2007925117, 2020.

521 Convey, P. and McInnes, S. J.: Exceptional tardigrade-dominated ecosystems in Ellsworth Land, Antarctica, *Ecology*, 86(2),
522 519–527, doi:10.1890/04-0684, 2005.

523 Courtright, E. M., Wall, D. H. and Virginia, R. A.: Determining habitat suitability for soil invertebrates in an extreme
524 environment: The McMurdo Dry Valleys, Antarctica, *Antarct. Sci.*, 13(1), 9–17, doi:10.1017/S0954102001000037, 2001.

525 Davidson, A. D., Hamilton, M. J., Boyer, A. G., Brown, J. H. and Ceballos, G.: Multiple ecological pathways to extinction in
526 mammals., 2009.

527 Diaz, M. A., Adams, B. J., Welch, K. A., Welch, S. A., Opiyo, S. O., Khan, A. L., McKnight, D. M., Cary, S. C. and Lyons,
528 W. B.: Aeolian Material Transport and Its Role in Landscape Connectivity in the McMurdo Dry Valleys, Antarctica, *J.*
529 *Geophys. Res. Earth Surf.*, 123, 3323–3337, doi:10.1029/2017JF004589, 2018.

530 Diaz, M. A., Corbett, L. B., Bierman, P. R., Adams, B. J., Wall, D. H., Hogg, I. D., Fierer, N. and Lyons, W. B.: Relative
531 terrestrial exposure ages inferred from meteoric ¹⁰Be and NO₃- concentrations in soils along the Shackleton Glacier,
532 Antarctica, *Earth Surf. Dyn.*, in review, doi:https://doi.org/10.5194/esurf-2020-50, 2020a.

533 Diaz, M. A., Li, J., Michalski, G., Darrah, T. H., Adams, B. J., Wall, D. H., Hogg, I. D., Fierer, N., Welch, S. A., Gardner, C.
534 B. and Lyons, W. B.: Stable isotopes of nitrate, sulfate, and carbonate in soils from the Transantarctic Mountains, Antarctica:
535 A record of atmospheric deposition and chemical weathering, *Front. Earth Sci.*, 8(341), doi:10.3389/feart.2020.00341,
536 2020b.

537 Dragone, N. B., Diaz, M. A., Hogg, I., Lyons, W. B., Jackson, W. A., Wall, D. H., Adams, B. J. and Fierer, N.: Exploring the
538 boundaries of microbial habitability in soil, *bioRxiv*, doi:https://doi.org/10.1101/2020.08.03.234583, 2020.

539 Freckman, D. W. and Virginia, R. A.: Soil Biodiversity and Community Structure in the McMurdo Dry Valleys, Antarctica,
540 in *Ecosystem dynamics in a polar desert; the McMurdo dry valleys, Antarctica*, edited by J. C. Prisco, pp. 323–335,
541 American Geophysical Union (AGU), 1998.

542 Golledge, N. R. and Levy, R. H.: Geometry and dynamics of an East Antarctic Ice Sheet outlet glacier, under past and
543 present climates, *J. Geophys. Res.*, 116(F3), F03025, doi:10.1029/2011JF002028, 2011.

544 Golledge, N. R., Fogwill, C. J., Mackintosh, A. N. and Buckley, K. M.: Dynamics of the last glacial maximum Antarctic ice-
545 sheet and its response to ocean forcing, *Proc. Natl. Acad. Sci. U. S. A.*, 109(40), 16052–16056, doi:10.1073/pnas.1, 2012.

546 Golledge, N. R., Levy, R. H., McKay, R. M., Fogwill, C. J., White, D. A., Graham, A. G. C., Smith, J. A., Hillenbrand, C.
547 D., Licht, K. J., Denton, G. H., Ackert, R. P., Maas, S. M. and Hall, B. L.: Glaciology and geological signature of the Last
548 Glacial Maximum Antarctic ice sheet, *Quat. Sci. Rev.*, 78, 225–247, doi:10.1016/j.quascirev.2013.08.011, 2013.

549 Heindel, R. C., Spickard, A. M. and Virginia, R. A.: Landscape-scale soil phosphorus variability in the McMurdo Dry
550 Valleys, *Antarct. Sci.*, 29(3), 252–263, doi:10.1017/S0954102016000742, 2017.

551 Heung, B., Bulmer, C. E. and Schmidt, M. G.: Predictive soil parent material mapping at a regional-scale: A Random Forest
552 approach, *Geoderma*, 214–215, 141–154, doi:10.1016/j.geoderma.2013.09.016, 2014.

553 Hodgson, D. A., Convey, P., Verleyen, E., Vyverman, W., McInnes, S. J., Sands, C. J., Fernández-Carazo, R., Willemotte, A.,
554 De Wever, A., Peeters, K., Tavernier, I. and Willems, A.: The limnology and biology of the Dufek Massif, Transantarctic
555 Mountains 82° South, *Polar Sci.*, 4(2), 197–214, doi:10.1016/j.polar.2010.04.003, 2010.

556 Hogg, I. D. and Wall, D. H.: Polar deserts, in *Life at Extremes: Environments, Organisms and Strategies for Survival*, edited
557 by E. M. Bell, pp. 176–195, CAB International., 2012.

558 Howat, I. M., Porter, C., Smith, B. E., Noh, M.-J. and Morin, P.: The Reference Elevation Model of Antarctica, *Cryosph.*,
559 13, 665–674, doi:10.5194/tc-13-665-2019, 2019.

560 Jackson, A., Davila, A. F., Böhlke, J. K., Sturchio, N. C., Sevanthi, R., Estrada, N., Brundrett, M., Lacelle, D., McKay, C. P.,
561 Poghosyan, A., Pollard, W. and Zacny, K.: Deposition, accumulation, and alteration of Cl⁻, NO₃⁻, ClO₄⁻ and ClO₃⁻ salts in
562 a hyper-arid polar environment: Mass balance and isotopic constraints, *Geochim. Cosmochim. Acta*, 182, 197–215,
563 doi:10.1016/j.gca.2016.03.012, 2016.

564 Jackson, M. S., Hall, B. L. and Denton, G. H.: Asynchronous behavior of the Antarctic Ice Sheet and local glaciers during
565 and since Termination 1, Salmon Valley, Antarctica, *Earth Planet. Sci. Lett.*, 482, 396–406, doi:10.1016/j.epsl.2017.11.038,
566 2018.

567 Jackson, W. A., Davila, A. F., Estrada, N., Lyons, W. B., Coates, J. D. and Priscu, J. C.: Perchlorate and chlorate
568 biogeochemistry in ice-covered lakes of the McMurdo Dry Valleys, Antarctica, *Geochim. Cosmochim. Acta*, 98, 19–30,
569 doi:10.1016/j.gca.2012.09.014, 2012.

570 Jackson, W. A., Böhlke, J. K., Andraski, B. J., Fahlquist, L., Bexfield, L., Eckardt, F. D., Gates, J. B., Davila, A. F., McKay,
571 C. P., Rao, B., Sevanthi, R., Rajagopalan, S., Estrada, N., Sturchio, N., Hatzinger, P. B., Anderson, T. A., Orris, G.,
572 Betancourt, J., Stonestrom, D., Latorre, C., Li, Y. and Harvey, G. J.: Global patterns and environmental controls of
573 perchlorate and nitrate co-occurrence in arid and semi-arid environments, *Geochim. Cosmochim. Acta*, 164, 502–522,
574 doi:10.1016/J.GCA.2015.05.016, 2015.

575 Kassambara, A. and Mundt, F.: Package “factoextra,” *Extr. Vis. results Multivar. data Anal.*, 76 [online] Available from:
576 <https://github.com/kassambara/factoextra/issues> (Accessed 11 August 2020), 2017.

577 Kirkwood, C., Cave, M., Beamish, D., Grebby, S. and Ferreira, A.: A machine learning approach to geochemical mapping, *J.*
578 *Geochemical Explor.*, 167, 49–61, doi:10.1016/j.gexplo.2016.05.003, 2016.

579 LaPrade, K. E.: Climate, geomorphology, and glaciology of the Shackleton Glacier area, Queen Maud Mountains,
580 Transantarctic Mountains, Antarctica, *Antarct. Res. Ser.*, 36(9), 163–196, doi:10.1029/ar036p0163, 1984.

581 Levy, J. S., Fountain, A. G., Welch, K. A. and Lyons, W. B.: Hypersaline “wet patches” in Taylor Valley, Antarctica,
582 *Geophys. Res. Lett.*, 39(5), n/a-n/a, doi:10.1029/2012GL050898, 2012.

583 Lyons, W. B., Welch, K. A., Neumann, K., Toxey, J. K., McArthur, R., Williams, C., McKnight, D. M. and Moorhead, D.
584 L.: Geochemical linkages among glaciers, streams and lakes within the Taylor Valley, Antarctica, *Ecosyst. Dyn. a polar*
585 *desert; McMurdo dry Val. Antarct.*, 72, 77–92, doi:10.1029/AR072p0077, 1998.

586 Lyons, W. B., Deuerling, K., Welch, K. A., Welch, S. A., Michalski, G., Walters, W. W., Nielsen, U., Wall, D. H., Hogg, I.
587 and Adams, B. J.: The Soil Geochemistry in the Beardmore Glacier Region, Antarctica: Implications for Terrestrial
588 Ecosystem History, *Sci. Rep.*, 6, 26189, doi:10.1038/srep26189, 2016.

589 Magalhães, C., Stevens, M. I., Cary, S. C., Ball, B. A., Storey, B. C., Wall, D. H., Türk, R. and Ruprecht, U.: At Limits of
590 Life: Multidisciplinary Insights Reveal Environmental Constraints on Biotic Diversity in Continental Antarctica, edited by F.
591 de Bello, *PLoS One*, 7(9), e44578, doi:10.1371/journal.pone.0044578, 2012.

592 Nakada, M. and Lambeck, K.: The melting history of the late Pleistocene Antarctic ice sheet., 1988.

593 Nkem, J. N., Virginia, A. R. A., Barrett, A. J. E., Wall, D. H. and Li, A. G.: Salt tolerance and survival thresholds for two
594 species of Antarctic soil nematodes, *Polar Biol.*, 29, 643–651, doi:10.1007/s00300-005-0101-6, 2006.

595 Patel, J., Shah, S., Thakkar, P. and Kotecha, K.: Predicting stock market index using fusion of machine learning techniques,
596 *Expert Syst. Appl.*, 42(4), 2162–2172, doi:10.1016/j.eswa.2014.10.031, 2015.

597 Peters, J., De Baets, B., Verhoest, N. E. C., Samson, R., Degroeve, S., Becker, P. De and Huybrechts, W.: Random forests as
598 a tool for ecohydrological distribution modelling, *Ecol. Modell.*, 207(2–4), 304–318, doi:10.1016/j.ecolmodel.2007.05.011,
599 2007.

600 Prasad, A. M., Iverson, L. R. and Liaw, A.: Newer classification and regression tree techniques: Bagging and random forests
601 for ecological prediction, *Ecosystems*, 9(2), 181–199, doi:10.1007/s10021-005-0054-1, 2006.

602 R Core Team: *R: A language and environment for statistical computing*, 2020.

603 Scarrow, J. W., Balks, M. R. and Almond, P. C.: Three soil chronosequences in recessional glacial deposits near the polar
604 plateau, in the Central Transantarctic Mountains, Antarctica, *Antarct. Sci.*, 26(5), 573–583,
605 doi:10.1017/S0954102014000078, 2014.

606 Stafoggia, M., Bellander, T., Bucci, S., Davoli, M., de Hoogh, K., de' Donato, F., Gariazzo, C., Lyapustin, A., Michelozzi,
607 P., Renzi, M., Scortichini, M., Shtein, A., Viegi, G., Kloog, I. and Schwartz, J.: Estimation of daily PM10 and PM2.5
608 concentrations in Italy, 2013–2015, using a spatiotemporal land-use random-forest model, *Environ. Int.*, 124, 170–179,
609 doi:10.1016/j.envint.2019.01.016, 2019.

610 Stevens, M. I. and Hogg, I. D.: Long-term isolation and recent range expansion from glacial refugia revealed for the endemic
611 springtail *Gomphiocephalus hodgsoni* from Victoria Land, Antarctica, *Mol. Ecol.*, 12(9), 2357–2369, doi:10.1046/j.1365-
612 294X.2003.01907.x, 2003.

613 Stevens, M. I., Greenslade, P., Hogg, I. D. and Sunnucks, P.: Southern Hemisphere Springtails: Could Any Have Survived
614 Glaciation of Antarctica?, *Mol. Biol. Evol.*, 23(5), 874–882, doi:10.1093/molbev/msj073, 2006.

615 Talarico, F. M., McKay, R. M., Powell, R. D., Sandroni, S. and Naish, T.: Late Cenozoic oscillations of Antarctic ice sheets
616 revealed by provenance of basement clasts and grain detrital modes in ANDRILL core AND-1B, *Glob. Planet. Change*, 96–
617 97, 23–40, doi:10.1016/j.gloplacha.2009.12.002, 2012.

618 Tesoriero, A. J., Gronberg, J. A., Juckem, P. F., Miller, M. P. and Austin, B. P.: Predicting redox-sensitive contaminant
619 concentrations in groundwater using random forest classification, *Water Resour. Res.*, 53(8), 7316–7331,
620 doi:10.1002/2016WR020197, 2017.

621 Toner, J. D., Sletten, R. S. and Prentice, M. L.: Soluble salt accumulations in Taylor Valley, Antarctica: Implications for
622 paleolakes and Ross Sea Ice Sheet dynamics, *J. Geophys. Res. Earth Surf.*, 118(1), 198–215, doi:10.1029/2012JF002467,
623 2013.

624 Wall, D. H., Bardgett, R. D., Behan-Pelletier, V., Herrick, J. E., Jones, H., Ritz, K., Six, J., Strong, D. R. and van der Putten,
625 W. H., Eds.: *Soil Ecology and Ecosystem Services*, Oxford University Press, Oxford., 2012.

626 Warton, D. I., Duursma, R. A., Falster, D. S. and Taskinen, S.: smatr 3- an R package for estimation and inference about
627 allometric lines, *Methods Ecol. Evol.*, 3(2), 257–259, doi:10.1111/j.2041-210X.2011.00153.x, 2012.

628 Webster-Brown, J., Gall, M., Gibson, J., Wood, S. and Hawes, I.: The biogeochemistry of meltwater habitats in the Darwin
629 Glacier region (80°S), Victoria Land, Antarctica, *Antarct. Sci.*, 22(6), 646–661, doi:10.1017/S0954102010000787, 2010.

630 Wilson, D. J., Bertram, R. A., Needham, E. F., van de Fliedert, T., Welsh, K. J., McKay, R. M., Mazumder, A., Riesselman,
631 C. R., Jimenez-Espejo, F. J. and Escutia, C.: Ice loss from the East Antarctic Ice Sheet during late Pleistocene interglacials,
632 *Nature*, 561(7723), 383–386, doi:10.1038/s41586-018-0501-8, 2018.

633 Zeglin, L. H., Sinsabaugh, R. L., Barrett, J. E., Gooseff, M. N. and Takacs-Vesbach, C. D.: Landscape Distribution of
634 Microbial Activity in the McMurdo Dry Valleys: Linked Biotic Processes, Hydrology, and Geochemistry in a Cold Desert
635 Ecosystem, *Ecosystems*, 12(4), 562–573, doi:10.1007/s10021-009-9242-8, 2009.

636